TISSUE ENGINEERING: Part A
Volume 20, Numbers 17 and 18, 2014

DOI: 10.1089/ten.tea.2013.0645

Microporous Dermal-Like Electrospun Scaffolds Promote Accelerated Skin Regeneration

Paul P. Bonvallet, BS,[1] Bonnie K. Culpepper, PhD,[2] Jennifer L. Bain, DMD, PhD,[3] Matthew J. Schultz, BS,[1] Steven J. Thomas, MD,[4] and Susan L. Bellis, PhD[1,2]

The goal of this study was to synthesize skin substitutes that blend native extracellular matrix (ECM) molecules with synthetic polymers which have favorable mechanical properties. To this end, scaffolds were electrospun from collagen I (col) and poly(ε-caprolactone) (PCL), and then pores were introduced mechanically to promote fibroblast infiltration, and subsequent filling of the pores with ECM. A 70:30 col/PCL ratio was determined to provide optimal support for dermal fibroblast growth, and a pore diameter, 160 μm, was identified that enabled fibroblasts to infiltrate and fill pores with native matrix molecules, including fibronectin and collagen I. Mechanical testing of 70:30 col/PCL scaffolds with 160 μm pores revealed a tensile strength of 1.4 MPa, and the scaffolds also exhibited a low rate of contraction (< 19%). Upon implantation, scaffolds should support epidermal regeneration; we, therefore, evaluated keratinocyte growth on fibroblast-embedded scaffolds with matrix-filled pores. Keratinocytes formed a stratified layer on the surface of fibroblast-remodeled scaffolds, and staining for cytokeratin 10 revealed terminally differentiated keratinocytes at the apical surface. When implanted, 70:30 col/PCL scaffolds degraded within 3–4 weeks, an optimal time frame for degradation *in vivo*. Finally, 70:30 col/PCL scaffolds with or without 160 μm pores were implanted into full-thickness critical-sized skin defects. Relative to nonporous scaffolds or sham wounds, scaffolds with 160 μm pores induced accelerated wound closure, and stimulated regeneration of healthy dermal tissue, evidenced by a more normal-appearing matrix architecture, blood vessel in-growth, and hair follicle development. Collectively, these results suggest that microporous electrospun scaffolds are effective substrates for skin regeneration.

Introduction

Skin is often damaged as a result of physical insult, burns, diabetic ulcers, and other traumatic events. Frequently, the wound can heal on its own; however, large wounds require surgical intervention. Current treatments for skin repair include the use of autograft, allograft, or xenograft tissues. Autografted skin is the gold standard therapy; however, the amount of donor skin is in limited supply, and the quality of donor skin is sometimes compromised. Allograft and xenograft tissues are substitutes for autograft; however, these materials present disadvantages such as graft rejection, scar formation, contraction, and potential disease transmission.[1,2] Accordingly, intensive research is aimed at developing synthetic skin-mimetic materials that serve as temporary supports, while simultaneously inducing the regeneration of native skin tissue.[3,4]

Many engineered skin substitutes incorporate molecules found within the native extracellular matrix (ECM). ECM is critical for the guidance of cells and proper tissue formation during the wound-healing process. Collagen I is an abundant dermal ECM molecule, and it is widely used in regenerative scaffolds. However, collagen-based materials often have inadequate tensile properties due to collagen's fast degradation rate and poor mechanical characteristics.[5] In order to circumvent this issue, collagen I is either chemically cross-linked or mixed with synthetic polymers that add mechanical strength and flexibility. Poly(ε-caprolactone) (PCL) is an FDA-approved degradable polymer that is commonly blended with collagen I to create scaffolds with a tunable degradation rate and increased tensile strength.[6] While many methods can be used to generate collagen/PCL composites, electrospinning is emerging as a promising technology. Electrospinning offers a simple method for producing scaffolds that can be tailored to mimic the biochemistry and three-dimensional structure of native ECM.[7] Electrospun scaffolds composed of PCL and collagen I support cell adhesion and proliferation, possess favorable biomechanical characteristics, have a high surface-to-volume ratio, and are composed of a nanofibrous structure with interconnected pores, similar to native ECM.[8–10]

Departments of [1]Cell, Developmental and Integrative Biology, [2]Biomedical Engineering, [3]Periodontology, and [4]Surgery, University of Alabama at Birmingham, Birmingham, Alabama.

One of the main limitations of electrospun scaffolds is that the pores created by the nanofibrous mesh have small diameters which impede cell infiltration, hindering scaffold remodeling and wound healing.[11–13] A number of reports have highlighted the importance of porosity within skin-mimetic materials in facilitating fibroblast, endothelial, and stem cell infiltration; nutrient transport for better graft survival; and neovascularization.[14–16] On the other hand, if pores are too large, cells may have a difficult time filling the void with ECM. Excessive porosity or large pore diameters may also compromise scaffold mechanical properties. The most effective pore diameter for tissue regeneration is likely to be influenced by other scaffold properties such as the presence of integrin ligands for cell attachment and migration (e.g., collagen), scaffold stiffness, and degradation characteristics (e.g., amenability to endogenous enzymatic or hydrolytic processes).

The goal of the current study was to develop an electrospun scaffold that integrates a number of features which are critical for effective tissue repair, including a cell-instructive biochemical composition; suitable mechanical properties and degradation rate; and pores of sufficient size to enable cell infiltration and scaffold remodeling. Electrospun scaffolds composed of collagen I/PCL blends with varying pore diameters were evaluated for fibroblast-directed ECM deposition. Pores were created mechanically, based on an adaptation of a device used in the cosmetics field to stimulate skin regeneration. Specifically, a paddle-like device composed of numerous micro-diameter needles (Dermastamp) creates small injuries in the facial skin, which, consequently, promotes wound healing. Modeling this process, pores were created in electrospun scaffolds with micro-diameter needles, and a pore size that supported ECM deposition was identified. Microporous scaffolds implanted into full-thickness skin wounds were found to promote more rapid skin regeneration than standard electrospun scaffolds. Compared with other technologies for increasing scaffold pore size, the generation of a commercial press device with a defined needle diameter offers a technically straightforward and cost-effective strategy for introducing well-controlled and reproducible pores in sheets of electrospun materials.

Materials and Methods

Preparation of electrospun scaffolds

One hundred percent PCL, 50:50 col/PCL, and 70:30 col/PCL scaffolds were synthesized by dissolving collagen I and PCL into hexafluoroisopropanol (HFP) solvent (Sigma), resulting in a solid weight of 7.5% of the total solution weight. Calf skin collagen I was purchased from MP Biomedicals, and 100,000 Da PCL was purchased from Scientific Polymer Products. Solutions were taken up into a 3-cc syringe with a 27-gauge needle, and a syringe pump (Harvard Apparatus) was used to eject the solution at a constant 2 mL/h rate toward an aluminum foil-covered collecting plate that rotated at 20 rotations/min. Scaffolds were placed in a desiccator for 24 h to remove any residual HFP. Individual scaffolds were punched from the larger electrospun sheet using a Humboldt Boring Machine (Fisher). Scaffolds were placed in CellCrowns (Scaffdex), and micropores were created mechanically using either an acupuncture needle (scaffolds with 160 μm pores) or a Dermastamp device (scaffolds with 250 μm pores, Dermastamp purchased from Alibaba.com). For cell culture studies, scaffolds were sterilized by soaking in 70% ethanol before use.

Cell culture

Immortalized J2 mouse fibroblasts were a generous gift from Louise Chow (University of Alabama at Birmingham [UAB]). Green fluorescent protein (GFP)-expressing J2 cells were generated by stable transduction with lentivirus particles obtained from the UAB Virology Core facility. GFP-J2 fibroblasts were cultured in Dulbecco's modified Eagle's medium that was supplemented with 10% fetal bovine serum (FBS) and 1% penicillin/streptomycin/amphotericin solution (Invitrogen). Primary human fibroblasts and keratinocytes harvested from neonatal foreskin were obtained from the Skin Cell Culture Core facility at UAB. Human fibroblasts were cultured in fibroblast basal medium that was supplemented with insulin, FBS, fibroblast growth factor, gentamicin, and amphotericin (Lonza). Keratinocytes were cultured in serum-free keratinocyte medium that was supplemented with L-glutamine, epidermal growth factor, and bovine pituitary extract (Gibco).

Cell growth on scaffolds

GFP expressing J2 fibroblasts were seeded onto scaffolds that were held in place by CellCrowns and allowed to grow for 3 or 10 days. Scaffolds were then removed from the CellCrowns, placed on microscope slides, and rinsed with phosphate-buffered saline (PBS). Cells were fixed in 4% paraformaldehyde for 15 min and permeabilized in 0.2% Triton-X 100 for 15 min. All steps were followed by three washes in PBS. The samples were coverslipped and imaged by confocal microscopy.

To quantitatively evaluate cell proliferation, 5×10^4 GFP-expressing J2 fibroblasts were seeded onto scaffolds and allowed to grow for varying time points ranging from 1 to 21 days. The samples were then rinsed in PBS, frozen in liquid nitrogen, and pulverized using a cryo-pulverizer. Cells were lysed in 50 mM Tris buffer (pH 7.4) containing 150 mM NaCl, 1% Triton X-100, 1% deoxycholate, 0.1% SDS, 5 mM EDTA, and 0.5% Igepal. Lysates were then homogenized and centrifuged at 15,000 *g* for 20 min at 4°C, and supernatants were collected for analysis. Solution fluorescence of the lysates (reflecting GFP) was measured using a BioRad Versafluor fluorometer. For western blotting, lysates were mixed with NuPAGE lithium dodecyl sulfate (LDS) and sample reducing agent (Invitrogen) and resolved in a BioRad precast gel at 100 V. The proteins were transferred overnight to a polyvinylidene fluoride (PVDF) membrane at 4°C. The membrane was blocked with 10% bovine serum albumin for an hour. An anti-GFP monoclonal antibody (Roche) and an HRP-conjugated secondary antibody (Cell Signaling) were used. Imaging was performed on a BioRad ChemiDoc imaging system.

Cell viability on scaffolds

Human fibroblasts (lacking any fluorescent tag) were seeded on the surface of scaffolds and allowed to grow for 1, 7, 14, and 21 days. Scaffolds containing fibroblasts were then submerged in a live/dead cell imaging solution for 15 min that

stains live cells green and dead cells red (Life Technologies). The scaffolds were subsequently imaged on a Nikon confocal microscope. Cell counting was performed by automatic detection using the Volocity image analysis software program in order to determine the number of live and dead cells.

Scanning electron microscopy of scaffolds

Scaffolds were dried in a desiccator for 24 h, gold plated, and imaged using a Philips XL-30 scanning electron microscopy with an accelerating voltage of 10 kV.

Cell invasion into pores and matrix deposition

Human fibroblasts were preloaded for 24 h with red fluorescent nanocrystals (Qtracker 655; Invitrogen), seeded onto scaffolds, and cultured for 10 days. Scaffolds were subsequently cut into strips, embedded in optimal cutting temperature (OCT) gel, frozen, and sectioned with a cryostat. Nuclei were stained with Hoechst. Matrix deposition was evaluated by phase-contrast imaging using a dissecting microscope, or scaffolds were stained for specific matrix molecules. Collagen was stained using a Picrosirius Red kit (Polysciences, Inc.), and fibronectin was detected using an anti-fibronectin antibody (Abcam), followed by Alexa-488 conjugated secondary antibody (Molecular Probes). Fibronectin and collagen deposition was validated by immunoblotting (primary antibodies from Abcam).

Keratinocyte stratification on fibroblast-remodeled scaffolds

Human fibroblasts were seeded on the scaffold surface and allowed to grow for 10 days. At this time point, human keratinocytes were seeded onto the fibroblast-embedded scaffolds and allowed to adhere for 24 h. Scaffolds were then placed on top of a wire mesh and media was filled to the level of the scaffold, positioning the keratinocyte layer at the air-media interface. Scaffolds were grown at the air–liquid interface for 10 days, and were then OCT embedded, frozen, and sectioned. Sections were stained with hematoxylin and eosin (H&E). In addition, scaffolds were immunostained for cytokeratin 10 (CK-10; Abcam).

Mechanical testing

Human foreskin fibroblasts were seeded onto 70:30 col/PCL scaffolds with or without mechanically generated pores and cultured for 7, 14, and 21 days. At each time point, the diameters of the scaffolds were measured with calipers. The difference in diameter from the original diameter was measured, and the percent contraction was calculated. The procedure was reproduced without seeded fibroblasts in order to compare the contraction of scaffolds with or without cells.

Tensile strength and strain were measured for scaffolds of varying col/PCL ratios, with or without 160 μm pores. The scaffolds were first soaked in PBS to ensure adequate hydration, and then, samples were analyzed using an MTS 858 mini Bionix mechanical test machine by applying a displacement strain rate of 5 mm/min, a time interval of 100 Hz, a 100-N load cell, and using MTS pneumatic controller grips. A dog-bone-shaped die was used to cut scaffolds. Scaffold thickness and grip distance were measured and taken into account before testing.

Degradation of scaffolds in vivo

All animal procedures were performed under the guidelines approved by the Institutional Animal Care and Use Committee (IACUC) at the University of Alabama at Birmingham. Three 15-mm-diameter full-thickness wounds were created in the backskin of a Sprague-Dawley rat (i.e., each rat received a total of three wounds placed linearly on the backskin). One of the wounds was implanted with a 70:30 col/PCL scaffold, another with a 50:50 col/PCL scaffold, and the third was covered with gauze (sham) ($n = 5$ rats). Scaffolds were stained with DiI dye (Invitrogen) before implantation. At 7, 14, and 26 days, tissues were harvested, OCT embedded, and sectioned. Fluorescent pictures were taken, and the areas of the remaining scaffold were measured using NIS Elements BR software.

Wound closure and histology

As described earlier, each rat received three 15 mm-diameter full-thickness wounds on the backskin. One wound was implanted with a 70:30 col/PCL scaffold containing 160 μm pores; the second wound was implanted with a 70:30 col/PCL scaffold lacking micropores; and the third wound was covered with gauze as a sham control ($n = 5$). Top-view photos of the rat backskin containing the three side-by-side wounds were taken at 7, 14, and 21 days, and unhealed wound areas were measured by Image J analysis. Tissues were harvested at these same time points, paraffin embedded, sectioned, and stained with H&E. Representative images were taken to highlight blood vessel formation, hair follicle development, and dermal matrix architecture. In addition, whole field H&E stained sections were taken with an Olympus VS120, and the junction between the normal and abnormal-appearing tissue was designated. The area of abnormal dermal tissue area was measured by Image J analysis.

Results

Fibroblast growth on scaffolds with varying ratios of collagen and PCL

Pilot studies were performed on electrospun scaffolds with varying collagen I/PCL ratios to identify a base formulation that supported fibroblast adhesion to the scaffold surface and subsequent cell proliferation. Four formulations were examined: (i) 100% collagen I; (ii) 70% collagen I and 30% PCL (70:30 col/PCL); (iii) 50% collagen I and 50% PCL (50:50 col/PCL); and (iv) 100% PCL. Scaffolds composed of 100% collagen I degraded within 24 h and were not investigated further. The three other scaffold formulations were seeded with GFP-expressing dermal fibroblasts, and cells were visualized by confocal microscopy (Fig. 1A). All three scaffolds supported some degree of cell attachment and survival, although at 10 days there appeared to be a greater number of cells on scaffolds composed of 70:30 col/PCL. Fibroblasts on the 70:30 col/PCL scaffolds displayed a well-spread morphology, and numerous mitotic figures were present (Fig. 1B), confirming active cell proliferation. Based on these data, further analyses of the 70:30 col/PCL scaffolds were performed. To quantitatively assess cell survival and proliferation, scaffolds with GFP-expressing fibroblasts were homogenized at varying time intervals and

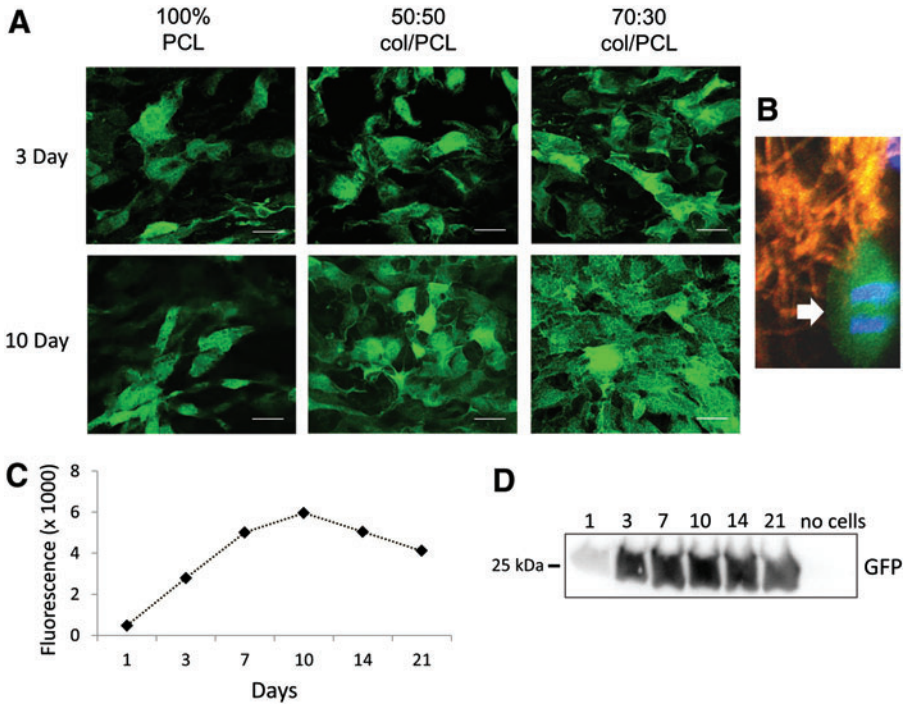

FIG. 1. Fibroblast growth and proliferation on electrospun scaffolds composed of varying ratios of collagen I and poly(ε-caprolactone) (PCL). **(A)** Green fluorescent protein (GFP)-expressing J2 fibroblasts were seeded onto scaffolds and allowed to grow for 3 or 10 days. Shown in the figure are representative images of cells grown on scaffolds of 100% PCL, 50% collagen I:50% PCL (50:50 col/PCL) and 70% collagen I:30% PCL (70:30 col/PCL). Scale bar = 40 μm. **(B)** Mitotic fibroblasts were apparent on 70:30 col/PCL scaffolds (arrow). In this experiment, the electrospun scaffold was stained with DiI dye to label scaffold fibers red. **(C)** GFP-expressing J2 fibroblasts were grown on 70:30 col/PCL scaffolds over a 21-day time interval, and cell lysates were prepared at designated time points. Fluorometer readings were taken from lysates. **(D)** Western Blot for GFP using lysates from the same samples used for fluorescence readings. As a negative control, homogenates were prepared from scaffolds lacking seeded fibroblasts (''no cells''). Each sample represents a pooled group of lysates from six distinct scaffolds, and two independent experiments were performed. Color images available online at www.liebertpub.com/tea

the fluorescence of the cell lysates (representing the GFP-expressing cell fraction) was measured by fluorometry (Fig. 1C). Cell lysates were also immunoblotted for GFP (Fig. 1D). A substantial increase in relative cell number was observed from 1 to 10 days, after which cell number stabilized. Stabilization is likely due to cells reaching confluence on the scaffold surface.

We next evaluated cell viability on 70:30 col/PCL scaffolds by seeding primary human fibroblasts (not expressing GFP) onto scaffolds, and then staining for both live (green) and dead (red) cells after 1, 7, 14, and 21 days. We observed minimal cell death over the 21 day time interval, and cells appeared to reach confluence between 7 and 14 days (Fig. 2A), consistent with results in Figure 1. The respective numbers of live and dead cells were quantified from multiple fields (Fig. 2B), which confirmed a low rate of cell death at each time point.

Optimization of scaffold pore size

Having determined that 70:30 col/PCL scaffolds provided good support for fibroblast growth, pores with diameters of either 250 or 160 μm were introduced into the scaffolds using microneedles (Fig. 3). Human dermal fibroblasts loaded with fluorescent nanocrystals were seeded onto the scaffolds and allowed to migrate and proliferate for 10 days. A confluent monolayer of fibroblasts formed on the surface of scaffolds with 250 and 160 μm diameter pores, indicating that sufficient fibroblast-mediated matrix deposition occurred to allow bridging across the top of the pores (Fig. 3C, F). However, it was evident that the 160, but not 250, μm pores were filled with matrix. We also compared the capacity of fibroblasts to fill the pores of scaffolds with varying col/PCL ratios. Fibroblasts were grown on either 70:30 or 50:50 col/PCL scaffolds with 160 μm pores, and at 7 days, minimal pore-filling was observed (Fig. 4A). However, at 14 days, there was obvious matrix deposition within the 70:30, but not 50:50, scaffolds. Magnified images at 14 days demonstrate that the newly deposited matrix was fibrous in nature. These results indicate that both the col/PCL ratio and pore diameter are important parameters for fibroblast-directed matrix deposition.

Infiltrating fibroblasts fill scaffold pores with ECM

Fibronectin is a major constituent in provisional wound-healing matrices,[17] therefore immunostaining for fibronectin was performed on the fibroblast-remodeled 70:30 col/PCL scaffolds with 160 μm pores. As shown in Figure 4B, a substantial amount of fibronectin was present throughout the pores. Scaffolds were also stained with picrosirius red, a dye selective for fibrillar forms of collagen (e.g., collagens I and III) that are abundantly secreted by fibroblasts. Extensive

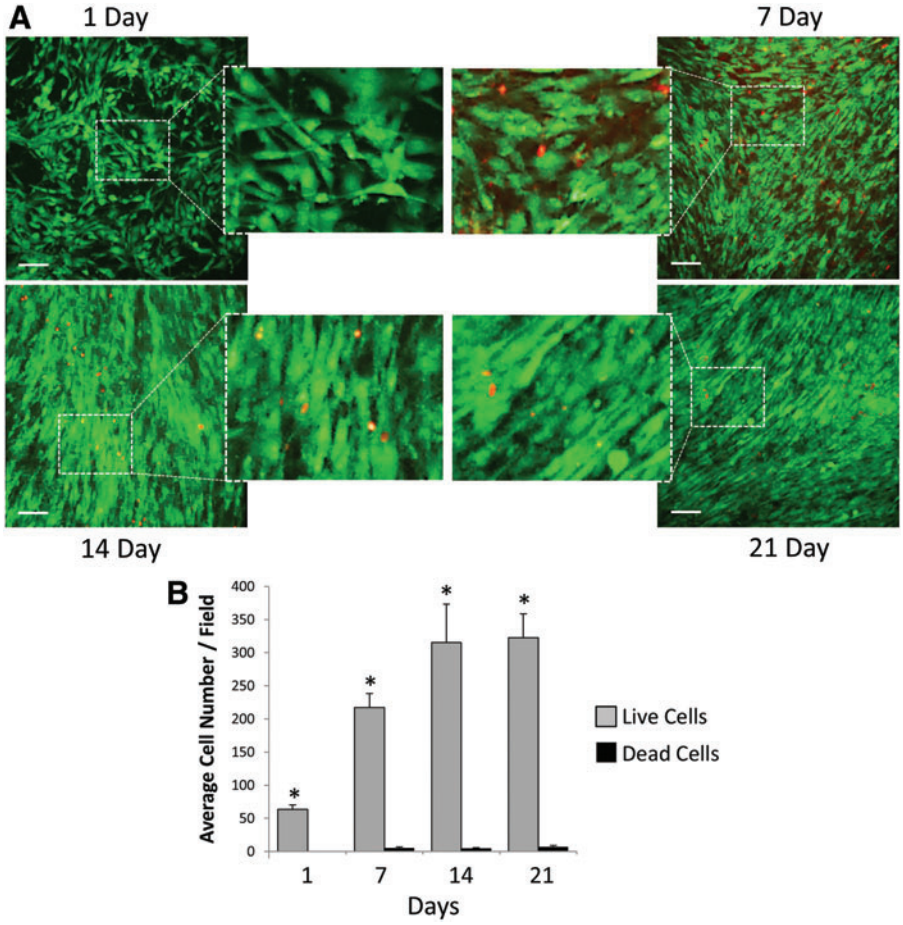

FIG. 2. Fibroblast viability on 70:30 col/PCL scaffolds. **(A)** Human fibroblasts (lacking GFP expression) grown on scaffolds for 1, 7, 14, or 21 days were stained for either living (green) or dead (red) cells. Scale bar = 90 μm. **(B)** Values represent means and standard error of the means measured for four distinct fields, detecting the amount of living and dead cells at each time point. Student's *t*-tests were used to compare the number of live cells versus the number of dead cells. *Represents significant difference ($p < 0.01$) relative to the dead cell number of the same day. Color images available online at www.liebertpub.com/tea

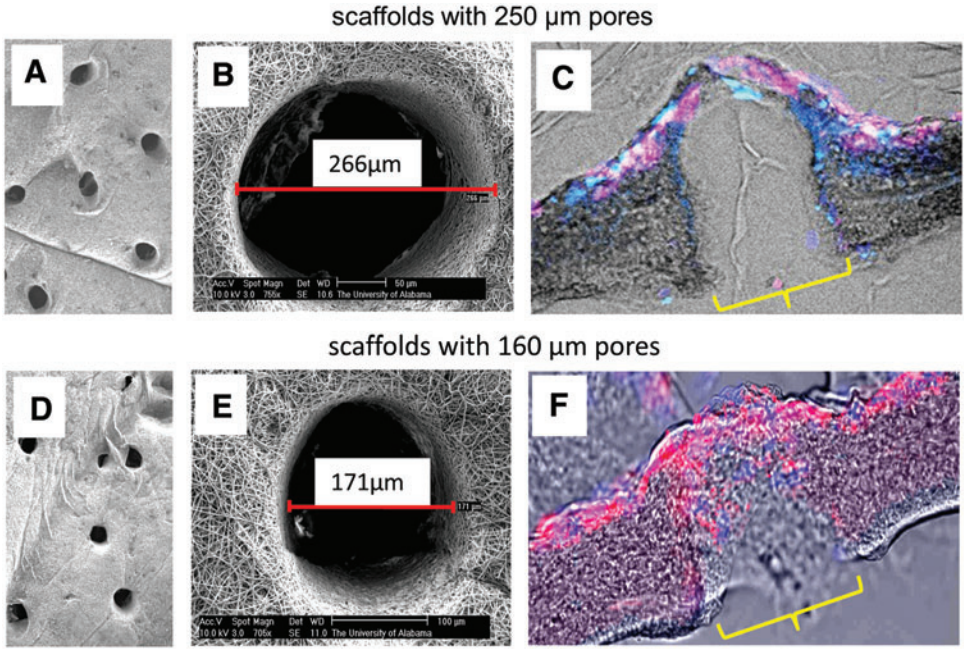

FIG. 3. Infiltrating fibroblasts fill 160 μm, but not 250 μm, pores with matrix. **(A, B)** Scanning electron microscopy (SEM) images of scaffolds with 250 μm pores. **(C)** Human dermal fibroblasts were preloaded with red fluorescent nanocrystals, and seeded onto porous scaffolds. Samples were counterstained with Hoescht. Fluorescent images were overlaid with phase-contrast images to show the scaffold area. **(D, E)** SEM images of scaffolds with 160 μm pores. **(F)** Fibroblasts loaded with red nanocrystals migrated into the 160 μm pores and deposited matrix. Samples were counterstained with Hoescht. Yellow brackets indicate a pore. Color images available online at www.liebertpub.com/tea

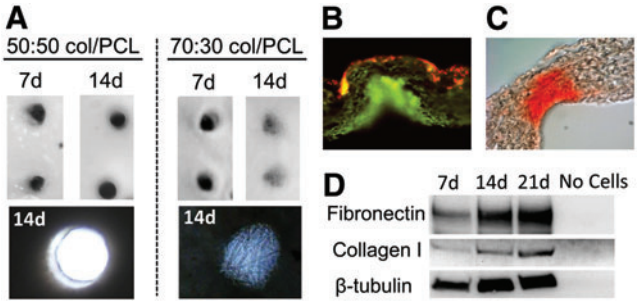

FIG. 4. Extracellular matrix is deposited into the pores of 70:30 col/PCL scaffolds, but not 50:50 col/PCL scaffolds. **(A)** Top view images of matrix deposition within pores at 7 and 14 days. Magnified images of 14-day samples reveal a fibrous matrix within pores of 70:30 col/PCL scaffolds. **(B)** Fibronectin deposition within 70:30 col/PCL scaffolds with 160 μm pores was detected by immunofluorescent staining (green). Red staining reflects fibroblasts preloaded with red nanocrystals. **(C)** Picrosirius Red was used to stain collagen in 70:30 col/PCL scaffolds with 160 μm pores. **(D)** Immunoblotting for fibronectin, collagen I, and β-tubulin was performed on homogenates prepared from microporous 70:30 col/PCL scaffolds with adherent fibroblasts grown for 7, 14, or 21 days. The ''no cells'' negative control homogenate was prepared from scaffolds that were not seeded with fibroblasts. Color images available online at www.liebertpub.com/tea

collagen deposition was observed (Fig. 4C). The deposition of collagen I and fibronectin was further validated by immunoblotting homogenates prepared from fibroblast-embedded scaffolds (Fig. 4D).

Scaffold mechanical properties

We next examined the effect of introducing pores on the mechanical properties of the scaffolds. Scaffolds with varying col/PCL ratios, with or without introduced pores, were analyzed for tensile strength and strain (Table 1). Comparable tensile strength and strain were observed for 70:30 and 50:50 col/PCL scaffolds, although both had lower values than 100% PCL. The addition of 160 μm pores had little effect on tensile strength for 100% PCL and 50:50 col/PCL scaffolds; however, strength of the microporous 70:30 col/PCL substrates was diminished to 1.4 MPa. Nonetheless, this value seems reasonable for therapeutic applications given that native skin exhibits a tensile strength of 5–30 MPa.[18]

Wound contraction is a natural part of healing; however, excessive contraction of dermal substitutes used for large wounds can lead to scarring, pain, and joint immobility. To address this issue, 70:30 col/PCL scaffolds with or without micropores were incubated in media over a 21-day time period and contraction was evaluated by measuring scaffold diameter (Fig. 5). Contraction occurred within the first 2 weeks for both scaffold types, and then stabilized. Scaffolds with micropores exhibited a maximal contraction of 18% within 21 days, while scaffolds without micropores had a 19% contraction. We subsequently evaluated contraction for scaffolds seeded with fibroblasts. Fibroblast-containing scaffolds without micropores had a maximal contraction rate of 17%, whereas microporous fibroblast-embedded scaffolds

Table 1. Tensile Testing of Porous and Nonporous Scaffolds

Scaffold	*Tensile strength (MPa)*	*Strain*
100% PCL—No pores	4.25 ± 0.96	0.44 ± 0.20[a]
100% PCL—Pores	4.32 ± 0.50	0.62 ± 0.03
50/50 col/PCL—No pores	2.87 ± 0.75	1.09 ± 0.25
50/50 col/PCL—Pores	2.90 ± 0.70	1.30 ± 0.15
70/30 col/PCL—No pores	2.17 ± 0.33[a]	1.14 ± 0.14[a]
70/30 col/PCL—Pores	1.40 ± 0.32	0.56 ± 0.16

Stress/strain values were calculated from tensile testing performed on scaffolds. Three different scaffold compositions, with or without pores, were evaluated. Values represent the means and standard deviation from six distinct scaffolds per group.

[a]Represents $p < 0.05$ compared with porous scaffolds of the same scaffold formulation.

PCL, poly(ε-caprolactone).

exhibited 13% contraction. These results demonstrate that the introduction of micropores into electrospun scaffolds does not increase the degree of scaffold contraction. Although one cannot directly compare with rates of scaffold contraction *in vivo*, the values observed for the microporous electrospun scaffolds seem acceptable, given that some clinical products have a contraction rate of approximately 50% when grafted.[19,20]

Fibroblast-remodeled scaffolds support keratinocyte growth and stratification

Re-epithelialization of the skin is a critical step in wound healing, and maturation of the epidermis is known to be dependent on a healthy supportive dermal layer.[21] Hence, we examined the capacity of fibroblast-embedded scaffolds

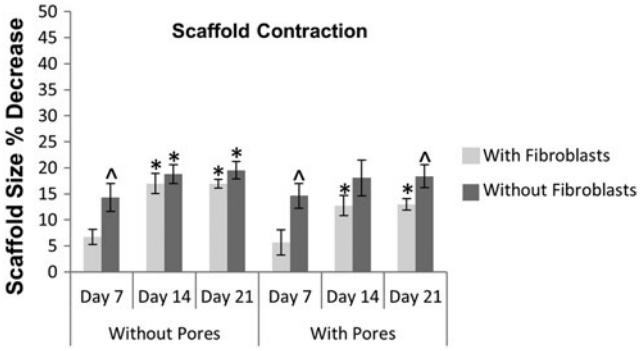

FIG. 5. Contraction of 70:30 col/PCL scaffolds with or without 160 μm pores and fibroblasts. Scaffolds were seeded with fibroblasts, and scaffold diameters were measured at varying time intervals to quantify contraction. The same experiment was also performed without seeded fibroblasts. Values represent means and standard deviation for five scaffolds per group, and two independent experiments were performed. Student's *t*-tests were used to compare the percent change in scaffold contraction of the various groups. *Represents significant difference ($p < 0.01$) relative to 7 day sample of the same group. ^Represents significant difference ($p < 0.05$) compared with scaffolds with fibroblasts for the same time point.

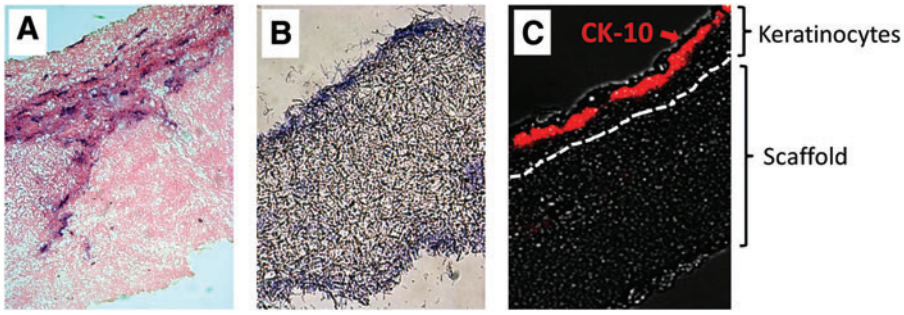

FIG. 6. Keratinocytes proliferate and form a stratified epidermal layer on the surface of fibroblast-remodeled scaffolds. **(A)** Fibroblast-remodeled 70:30 col/PCL scaffolds with 160 μm pores were seeded with keratinocytes and allowed to grow at the air–liquid interface for 10 days. Samples were stained with hematoxylin and eosin (H&E) to reveal the epidermal layer. **(B)** 70:30 col/PCL microporous scaffolds lacking fibroblasts were seeded with keratinocytes and grown at the air–liquid interface for 10 days. H&E staining showed that keratinocytes do not stratify on the surface of scaffolds without embedded fibroblasts. **(C)** Fibroblast-remodeled scaffolds with an overlying keratinocyte layer were immunostained for cytokeratin 10 (CK-10) (red), a marker for terminally differentiated keratinocytes. Color images available online at www.liebertpub.com/tea

to support keratinocyte growth. 70:30 col/PCL scaffolds with 160 μm pores were seeded with dermal fibroblasts, and the constructs were cultured for 10 days to enable matrix deposition. Keratinocytes were then seeded onto the surface of the scaffolds, and the substrates were grown at the air/media interface for an additional 10 days. H&E staining (Fig. 6A) suggested that keratinocytes proliferated and formed a stratified epidermal layer on top of the microporous scaffold surface. Conversely, keratinocytes grown on microporous 70:30 col/PCL scaffolds without embedded fibroblasts did not proliferate or stratify (Fig. 6B). To better characterize the effects of the fibroblast-remodeled scaffolds on maturation of the keratinocyte layer, fibroblast-embedded constructs with an overlying keratinocyte layer (prepared as in Fig. 6A) were immunostained for expression of CK-10, a marker for well-differentiated keratinocytes. CK-10 expression was found selectively in the apical surface of the keratinocyte layer, consistent with normal keratinocyte differentiation (Fig. 6C). Thus, keratinocytes grown on fibroblast-remodeled scaffolds recapitulate the normal cellular distribution and morphology of native epidermis.

Scaffold degradation and integration in vivo

Scaffolds are initially utilized as a support and an infrastructure for the guidance of new tissue development. However, as more mature skin tissue forms, scaffolds should degrade within 3–4 weeks to avoid hindering complete tissue healing.[22] To measure scaffold degradation rate, 50:50 and 70:30 col/PCL scaffolds (acellular) were prestained with a red fluorescent dye, and implanted into full-thickness skin wounds created in the backskin of rats. Fluorescent and phase-contrast images were taken of cross-sections from wounded tissues. NIS Elements BR software was used to quantify the area of scaffold remaining in the wound site. As shown in Figure 7, the 70:30 col/PCL scaffolds degraded more rapidly than 50:50 col/PCL scaffolds, with 70:30 col/PCL scaffolds exhibiting nearly complete degradation by 26 days. There appeared to be faster integration of 70:30 col/PCL scaffolds into the native tissue. These results suggest that 70:30 col/PCL scaffolds are incorporated into newly formed skin tissue and degrade within an optimal time interval for a skin substitute.

Porous scaffolds promote faster wound closure than scaffolds lacking micropores

Earlier studies suggested that 70:30 col/PCL scaffolds with 160 μm pores provided the best balance between biochemical composition, biomechanics, and biodegradability, and a permissive pore diameter for fibroblast infiltration and cell-directed matrix synthesis. We, thus, examined the efficacy of the scaffolds in stimulating wound healing. Three full-thickness critical-sized wounds were created in the backskin of a rat. One was implanted with a 70:30 col/PCL scaffold with 160 μm pores, another with a 70:30 col/PCL scaffold lacking micropores, and the third wound was covered with gauze (sham). Images were taken of the surface of the skin to monitor the rate of wound closure ($n = 5$, representative image shown in Fig. 8A). Wound closure was quantified at 7 and 14 days by measuring the area of unhealed tissue. Data were normalized by comparing the area of the scaffold-containing wound to the area of the corresponding sham wound for each animal. At 7 days after implantation, the amount of unhealed tissue associated with scaffolds lacking micropores, relative to the sham, was 97%, indicating that these scaffolds had a minimal effect on wound healing (''no-pores:sham ratio,'' Fig. 8B). In contrast, the amount of unhealed tissue present in wounds with porous scaffolds, relative to sham, was 67% at 7 days (''pores:sham ratio,'' Fig. 8B). Strikingly, the no-pores:sham ratio of unhealed tissue remained at 97% at 14 days (Fig. 8C), underscoring the poor performance of electrospun scaffolds with insufficient porosity. For the wounds with microporous scaffolds, the unhealed tissue area had decreased further to 40% at 14 days (relative to shams) (Fig. 8C).

Microporous scaffolds facilitate regeneration of more normal-appearing skin tissue

Scaffolds were implanted into full-thickness critical-sized skin wounds, and tissues were harvested for histology at 7,

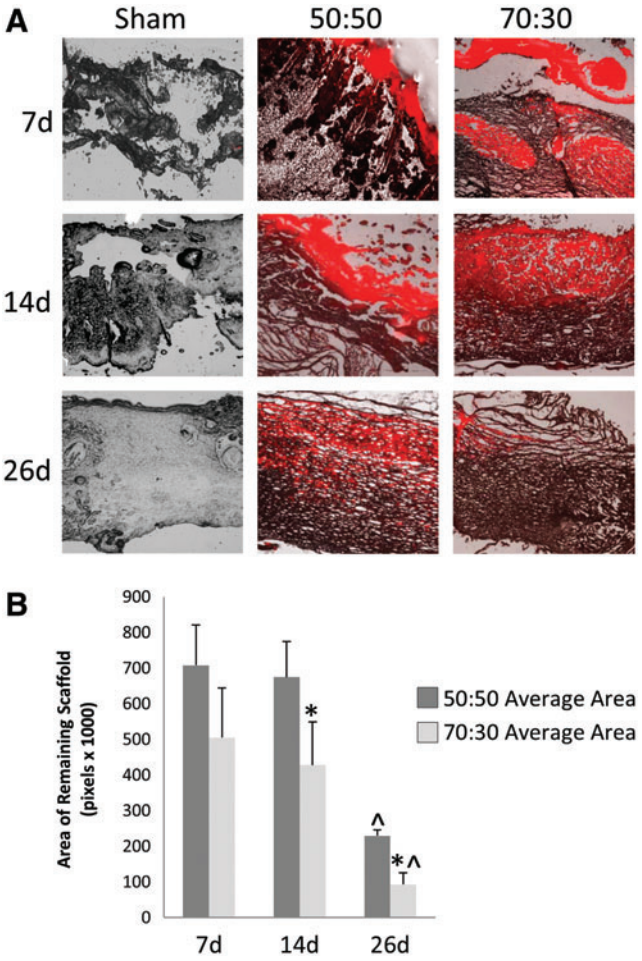

FIG. 7. 70:30 col/PCL scaffolds degrade more rapidly than 50:50 col/PCL scaffolds. **(A)** Scaffolds were stained a fluorescent red with DiI and implanted into rat full-thickness skin wound defects. At 7, 14, and 26 days, tissue was harvested, sectioned, and imaged to assess degradation ($n=5$). **(B)** The area of the remaining fluorescent scaffold was analyzed using NIS Elements software. Student's *t*-tests were used to compare the area of remaining scaffold of the various groups for all time points. *Significantly different ($p<0.05$) than 50:50 scaffolds of the same day. ^Significantly different ($p<0.05$) than 7 and 14 days of the same group. Color images available online at www.liebertpub.com/tea

14, and 21 days. H&E staining of the sham wounds showed a dense matrix, absent of follicles or other structures, consistent with scar tissue formation. For the wounds implanted with scaffolds with or without micropores, as well as the shams, the junction between the normal-appearing skin and abnormal scar-like tissue was designated (Fig. 9A), and the area of abnormal tissue was quantified (Fig. 9B). The area of abnormal tissue was significantly smaller at every time point in wounds implanted with 70:30 scaffolds with 160 μm pores as compared with scaffolds lacking micropores, or the shams.

We also examined higher-magnification images to better assess the quality of the newly formed tissue. Defects implanted with 70:30 col/PCL scaffolds with 160 μm pores supported the rapid formation of an overlying epidermal layer with finger-like projections into the dermis, which function to strengthen the bond between the two layers of skin (Fig. 10). It also appeared that microporous scaffolds facilitated earlier infiltration of new blood vessels when compared with defects implanted with standard electrospun scaffolds or the shams. Another notable feature was the architecture of the matrix. The newly formed matrix within defects implanted with the microporous scaffolds had a loose, wavy appearance, similar to native skin (Fig. 11). Conversely, the matrix within defects implanted with scaffolds lacking micropores or shams was markedly more compact. Finally, regenerated hair follicles were more numerous in wounds implanted with the microporous scaffolds (Figs. 10 and 11 and Table 2). These collective results suggest that electrospun scaffolds with micropores not only accelerate wound healing, but also stimulate greater regeneration of tissue approximating normal skin.

Discussion

There are numerous commercial skin graft products, along with many in the research phase, intended for use in the regeneration of damaged tissue.[6,23,24] However, an ideal skin graft material has yet to be developed.[2] Allogeneic or xenograft materials can elicit clinical challenges such as rejection, contraction, bleeding and infection, scar formation, and poor tissue formation,[1,2] whereas synthetic skin substitutes often lack sufficient biologic information for effective scaffold integration. An optimal bioengineered skin equivalent should assimilate a number of critical features such as appropriate three-dimensional architecture, tensile properties, degradation kinetics, and cell-instructive biochemical cues.[6]

Electrospinning is emerging as a promising approach for synthesizing regenerative scaffolds due to the (i) relatively low cost and simplicity of this technology; (ii) high capacity for blending multiple types of molecules within an ECM-like nanofibrous architecture; and (iii) tunable control of scaffold biomechanics and degradation rate. A wealth of literature has highlighted the suitability of electrospun scaffolds to serve as supports for cells that are integral to tissue repair, such as dermal fibroblasts or mesenchymal stem cells.[3,25–29] However, the small pores created by the electrospinning process restrict cell infiltration and scaffold remodeling. In the current study, scaffolds were electrospun with varying ratios of collagen I and PCL to identify a formulation, 70:30 col/PCL, that provided the best support for fibroblast growth, while maintaining sufficient tensile strength, low contractility, and a suitable degradation rate. Subsequently, pores were created mechanically, and an optimal pore diameter, 160 μm, was identified that enabled fibroblast infiltration and complete filling of the pores with fibroblast-secreted ECM molecules, including fibronectin and collagen I. Functionality of fibroblast-remodeled 70:30 col/PCL porous scaffolds was evidenced by the finding that keratinocytes cultured on the scaffold surface differentiated and formed a stratified epidermal layer.

When implanted into critical-sized full-thickness skin defects, 70:30 col/PCL scaffolds with 160 μm pores stimulated more rapid and effective wound healing compared with scaffolds lacking micropores or sham wounds. Wound closure was accelerated in defects with the porous scaffolds,

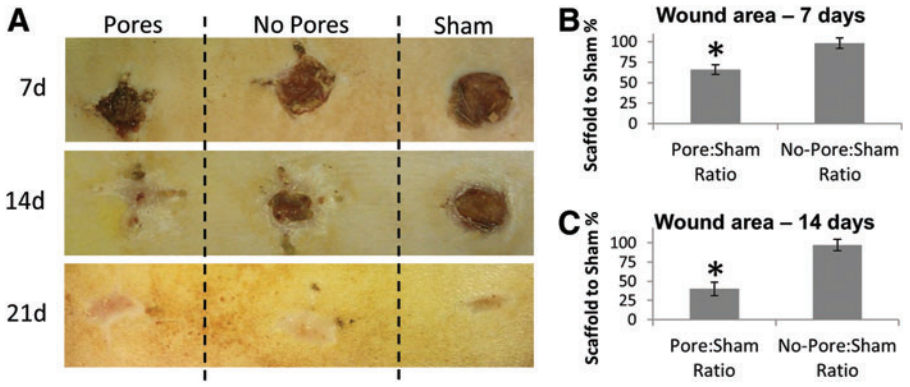

FIG. 8. More rapid wound closure is observed for critical-sized defects implanted with porous scaffolds. **(A)** Three side-by-side full-thickness wounds were created in the backskin of a rat. One wound was implanted with 70:30 col/PCL scaffolds with 160 μm pores (''Pores''), another wound was implanted with 70:30 col/PCL scaffolds lacking pores (''No Pores''), and the third wound was covered with gauze (''Sham''). Shown in the figure are representative images of the backskin of individual rats imaged at 7, 14, or 21 days after implantation. **(B, C)** The area of the unhealed wound at 7 and 14 days was measured with image J software, and values for the wounds implanted with scaffolds were normalized to the area of the sham for each animal ($n = 5$ animals). Student's t-tests were used to compare pores:sham ratio with no pores:sham ratio. *Significant difference ($p < 0.05$) relative to no pores:sham group. Color images available online at www.liebertpub.com/tea

and the quality of the regenerated tissue was more similar to native skin. In addition, a greater number of newly generated hair follicles were observed within wounds grafted with microporous scaffolds. Given that stem cells are required for the regeneration of hair follicles,[30] these data imply that stem cells were recruited from the surrounding unwounded skin tissue into the defect site. In the first week after wounding, greater neovascularization was apparent in tissues with implanted microporous scaffolds. Taken together, these results underscore the importance of pore size for proper tissue healing. Similar to our studies, Xiao *et al.* reported that pores created in acellular dermal matrix (ADM) from bovine skin were essential for the imbibition of plasma from the wound bed to the outer surface. The ADM was suggested to act as an inducer for the formation of a ''neodermis'' by the infiltration of fibroblasts and blood vessels.[14]

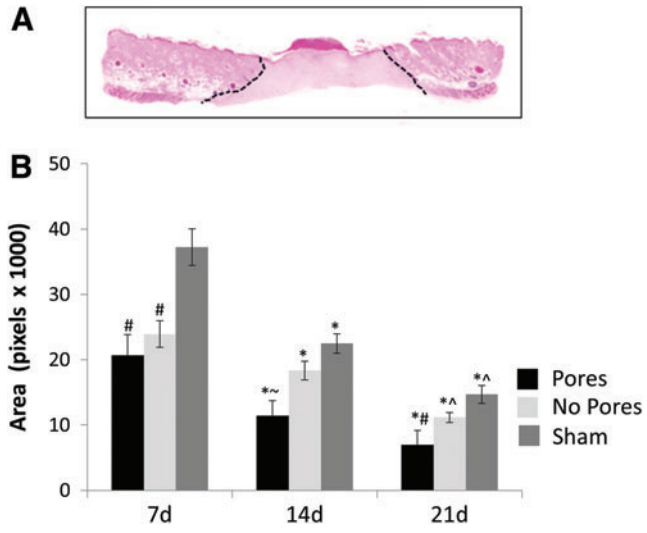

FIG. 9. Scaffolds with micropores promote more effective tissue regeneration. **(A)** Cross-section of rat skin tissue undergoing the wound-healing process. Black lines designate areas of abnormal tissue morphology. **(B)** Graph depicts average abnormal tissue areas for scaffolds with or without micropores or sham wounds. *Represents significant difference ($p < 0.01$) compared with day 7 of the respective group; ^represents significant difference ($p < 0.05$) relative to day 14 of the respective group; #represents significant difference ($p < 0.02$) relative to sham of the same day; and ~represents significant difference ($p < 0.05$) relative to sham and no pore samples of the same day. Error bars represent standard deviation. Color images available online at www.liebertpub.com/tea

Another advantage of scaffolds with mechanically generated pores is the feasibility for large-scale production. The use of a press-like device with microneedles is amenable to commercialization (as suggested by the Dermastamp device), and pores created in this manner have a homogeneous and well-defined size and spacing. A number of alternative electrospinning protocols have been developed to increase scaffold pore size[12,31–35]; however, these have primarily been successful with scaffolds composed solely of synthetic polymers. These variant protocols become more challenging when the scaffolds incorporate biologic molecules, which is noteworthy given the extensive evidence pointing to the importance of biologic molecules for optimal cell survival and signaling.[32,36,37] Moreover, it may be difficult to achieve good reproducibility of pore size and distribution when these alternate protocols are scaled up for commercial distribution. An additional benefit of the mechanically generated pores is that they are introduced after the synthesis of electrospun sheets. This approach would synergize with one of the key advantages of electrospinning, namely, the capacity to tailor scaffold biochemical composition to match tissue-specific ECMs. Mechanically created pores can be introduced into any type of electrospun formulation. For example, through the use of co-spinning from multiple syringes, additional fibers composed of molecules such as elastin can be incorporated,[38,39] while co-axial spinning can be employed to deliver various growth factors and

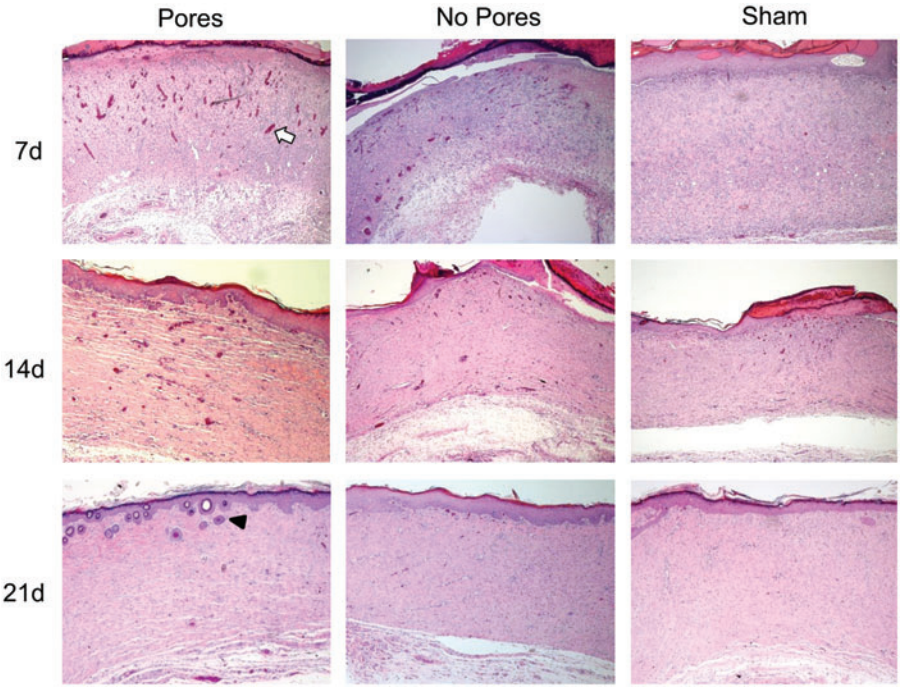

FIG. 10. Images (4×) of wound healing at 7, 14, and 21 days after implantation. Blood vessel formation is apparent in porous and nonporous 70:30 col/PCL scaffolds as early as 7 days (white arrow indicates a representative blood vessel). The epidermis in wounds containing 70:30 col/PCL scaffolds with 160 μm pores forms finger-like projections into the dermis, similar to normal unwounded epidermis. Hair follicle formation can also be seen in wounds containing microporous scaffolds (black arrowhead indicates a representative hair follicle). Color images available online at www.liebertpub.com/tea

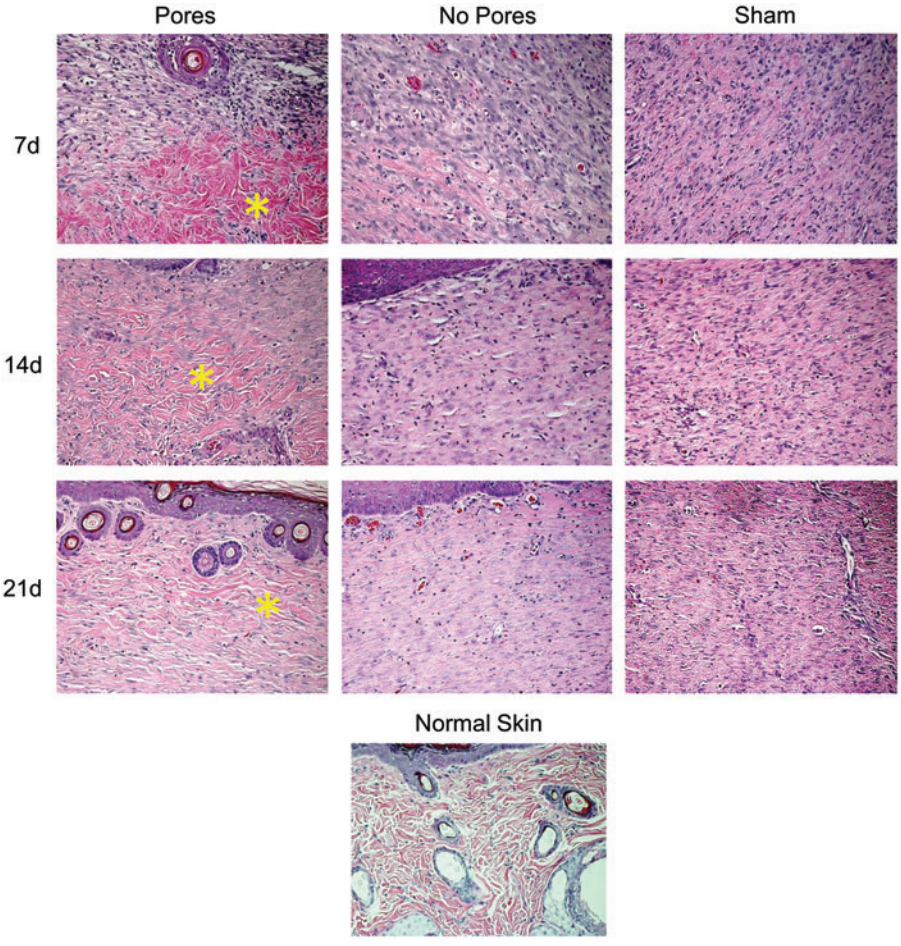

FIG. 11. Images (20×) of wound healing over a 21-day time period show the structure of the matrix. The structure of the matrix within wounds implanted with 70:30 col/PCL scaffolds with 160-μm pores appears more similar to normal skin, evidenced by a loose, wavy matrix (yellow asterisk) and the formation of new hair follicles. Color images available online at www.liebertpub.com/tea

Table 2. Number of Newly Formed Hair Follicles

Days	*Pores*	*No Pores*	*Sham*
7	15	10	0
14	29	13	5
21	56	21	9

The number of hair follicles was counted in different samples over a 21-day time frame. Five fields were chosen for each specimen, and the number of newly formed hair follicles was tallied ($n=5$ animals per group).

chemokines.[40,41] The mechanical generation of pores is compatible with these developing technologies, and it also offers a simpler and better-controlled strategy for increasing pore size when compared with methods such as the use of sacrificial fibers or particles.

In conclusion, 70:30 col/PCL scaffolds with 160 μm pores support dermal fibroblast infiltration and ECM deposition, and they also serve as favorable substrates for keratinocyte proliferation and stratification. When implanted into full-thickness skin wounds, the microporous scaffolds promote faster and better healing than scaffolds lacking micropores. These results not only establish the critical importance of scaffold pore diameter (even for scaffolds with uncrosslinked, cleavable collagen I), but also highlight a practical method for producing effective regenerative skin substitutes.

Acknowledgments

This research was supported by a grant from the Skin Diseases Research Center at the University of Alabama, Birmingham (NIH P30 AR050948). Bonvallet was supported by predoctoral fellowships funded by the NIH T32 training grant GM 008111-25, the National Center for Advancing Translational Research of the NIH TL1TR000167, and the Howard Hughes Medical Institute through the Med into Grad Initiative 56005705. Culpepper was supported by NIH/NIDCR predoctoral fellowship 1F31DE021613. The authors are grateful for assistance from the UAB Skin Cell Culture Core Facility, supported by NIH grant# P30 AR050948, the High Resolution Imaging Core Facility, the Experimental Biomechanics Core, and the Virology Core Facility.

Disclosure Statement

No competing financial interests exist.

References

1. Chern, P.L., Baum, C.L., and Arpey, C.J. Biologic dressings: current applications and limitations in dermatologic surgery. Dermatol Surg **35,** 891, 2009.
2. Priya, S.G., Jungvid, H., and Kumar, A. Skin tissue engineering for tissue repair and regeneration. Tissue Eng Part B Rev **14,** 105, 2008.
3. Jayarama Reddy, V., Radhakrishnan, S., Ravichandran, R., Mukherjee, S., Balamurugan, R., Sundarrajan, S., and Ramakrishna, S. Nanofibrous structured biomimetic strategies for skin tissue regeneration. Wound Repair Regen **21,** 11 2012.
4. Atala, A., Kasper, F.K., and Mikos, A.G. Engineering complex tissues. Sci Transl Med **4,** 160rv12, 2012.
5. Grover, C.N., Cameron, R.E., and Best, S.M. Investigating the morphological, mechanical and degradation properties of scaffolds comprising collagen, gelatin and elastin for use in soft tissue engineering. J Mech Behav Biomed Mater **10,** 62, 2012.
6. Zhong, S.P., Zhang, Y.Z., and Lim, C.T. Tissue scaffolds for skin wound healing and dermal reconstruction. Wiley Interdiscip Rev Nanomed Nanobiotechnol **2,** 510, 2010.
7. Kumbar, S.G., James, R., Nukavarapu, S.P., and Laurencin, C.T. Electrospun nanofiber scaffolds: engineering soft tissues. Biomed Mater **3,** 034002, 2008.
8. Venugopal, J., and Ramakrishna, S. Biocompatible nanofiber matrices for the engineering of a dermal substitute for skin regeneration. Tissue Eng **11,** 847, 2005.
9. Powell, H.M., and Boyce, S.T. Engineered human skin fabricated using electrospun collagen-PCL blends: morphogenesis and mechanical properties. Tissue Eng Part A **15,** 2177, 2009.
10. Cipitria, A., Skelton, A., Dargaville, T.R., Dalton, P.D., and Hutmacher, D.W. Design, fabrication and characterization of PCL electrospun scaffolds—a review. J Mater Chem **21,** 9419, 2011.
11. Kelleher, C.M., and Vacanti, J.P. Engineering extracellular matrix through nanotechnology. J R Soc Interface **7(Suppl 6),** S717, 2010.
12. Zhong, S., Zhang, Y., and Lim, C.T. Fabrication of large pores in electrospun nanofibrous scaffolds for cellular infiltration: a review. Tissue Eng Part B Rev **18,** 77, 2012.
13. Rnjak-Kovacina, J., and Weiss, A.S. Increasing the pore size of electrospun scaffolds. Tissue Eng Part B Rev **17,** 365, 2011.
14. Xiao, S.C., Xia, Z.F., Ben, D.F., Tang, H.T., Wang, G.Q., Zhu, S.H., and Yu, W.R. The role of pores in acellular dermal matrix substitute. Ann Burns Fire Disasters **19,** 192, 2006.
15. Wang, H.M., Chou, Y.T., Wen, Z.H., Wang, Z.R., Chen, C.H., and Ho, M.L. Novel biodegradable porous scaffold applied to skin regeneration. PLoS One **8,** e56330, 2013.
16. Chiu, Y.-C., Cheng, M.-H., Engel, H., Kao, S.-W., Larson, J.C., Gupta, S., and Brey, E.M. The role of pore size on vascularization and tissue remodeling in PEG hydrogels. Biomaterials **32,** 6045, 2011.
17. Kondo, T., and Ishida, Y. Molecular pathology of wound healing. Forensic Sci Int **203,** 93, 2010.
18. Li, W.J., Laurencin, C.T., Caterson, E.J., Tuan, R.S., and Ko, F.K. Electrospun nanofibrous structure: a novel scaffold for tissue engineering. J Biomed Mater Res **60,** 613, 2002.
19. Stephenson, A.J., Griffiths, R.W., and La Hausse-Brown, T.P. Patterns of contraction in human full thickness skin grafts. Br J Plast Surg **53,** 397, 2000.
20. Harrison, C.A., Gossiel, F., Layton, C.M., Bullock, A.J., Johnson, T., Blumsohn, A., and MacNeil, S. Use of an *in vitro* model of tissue-engineered skin to investigate the mechanism of skin graft contraction. Tissue Eng **12,** 3119, 2006.
21. Moulin, V., Auger, F.A., Garrel, D., and Germain, L. Role of wound healing myofibroblasts on re-epithelialization of human skin. Burns **26,** 3, 2000.
22. Franco, R., Nguyen, T., and Lee, B.-T. Preparation and characterization of electrospun PCL/PLGA membranes and

chitosan/gelatin hydrogels for skin bioengineering applications. J Mater Sci Mater Med **22,** 2207, 2011.
23. Philandrianos, C., Andrac-Meyer, L., Mordon, S., Feuerstein, J.M., Sabatier, F., Veran, J., Magalon, G., and Casanova, D. Comparison of five dermal substitutes in full-thickness skin wound healing in a porcine model. Burns **38,** 820, 2012.
24. van der Veen, V.C., Boekema, B.K., Ulrich, M.M., and Middelkoop, E. New dermal substitutes. Wound Repair Regen **19(Suppl 1),** s59, 2011.
25. Rnjak-Kovacina, J., Wise, S.G., Li, Z., Maitz, P.K., Young, C.J., Wang, Y., and Weiss, A.S. Tailoring the porosity and pore size of electrospun synthetic human elastin scaffolds for dermal tissue engineering. Biomaterials **32,** 6729, 2011.
26. Rnjak, J., Li, Z., Maitz, P.K., Wise, S.G., and Weiss, A.S. Primary human dermal fibroblast interactions with open weave three-dimensional scaffolds prepared from synthetic human elastin. Biomaterials **30,** 6469, 2009.
27. Gholipour-Kanani, A., Bahrami, S.H., Samadi-Kochaksaraie, A., Ahmadi-Tafti, H., Rabbani, S., Kororian, A., and Erfani, E. Effect of tissue-engineered chitosan-poly(vinyl alcohol) nanofibrous scaffolds on healing of burn wounds of rat skin. IET Nanobiotechnol **6,** 129, 2012.
28. Kim, H.L., Lee, J.H., Lee, M.H., Kwon, B.J., and Park, J.C. Evaluation of electrospun (1,3)-(1,6)-beta-D-glucans/biodegradable polymer as artificial skin for full-thickness wound healing. Tissue Eng Part A **18,** 2315, 2012.
29. Lu, L.X., Zhang, X.F., Wang, Y.Y., Ortiz, L., Mao, X., Jiang, Z.L., Xiao, Z., and Huang, N.P. Effects of hydroxyapatite-containing composite nanofibers on osteogenesis of mesenchymal stem cells *in vitro* and bone regeneration *in vivo*. ACS Appl Mater Interfaces **5,** 319, 2012.
30. Yang, C.C., and Cotsarelis, G. Review of hair follicle dermal cells. J Dermatol Sci **57,** 2, 2010.
31. Blakeney, B.A., Tambralli, A., Anderson, J.M., Andukuri, A., Lim, D.J., Dean, D.R., and Jun, H.W. Cell infiltration and growth in a low density, uncompressed three-dimensional electrospun nanofibrous scaffold. Biomaterials **32,** 1583, 2011.
32. Phipps, M.C., Clem, W.C., Grunda, J.M., Clines, G.A., and Bellis, S.L. Increasing the pore sizes of bone-mimetic electrospun scaffolds comprised of polycaprolactone, collagen I and hydroxyapatite to enhance cell infiltration. Biomaterials **33,** 524, 2012.
33. Zhu, X., Cui, W., Li, X., and Jin, Y. Electrospun fibrous mats with high porosity as potential scaffolds for skin tissue engineering. Biomacromolecules **9,** 1795, 2008.
34. Nam, J., Huang, Y., Agarwal, S., and Lannutti, J. Improved cellular infiltration in electrospun fiber via engineered porosity. Tissue Eng **13,** 2249, 2007.
35. Leong, M.F., Rasheed, M.Z., Lim, T.C., and Chian, K.S. *In vitro* cell infiltration and *in vivo* cell infiltration and vascularization in a fibrous, highly porous poly(D,L-lactide) scaffold fabricated by cryogenic electrospinning technique. J Biomed Mater Res A **91,** 231, 2009.
36. Phipps, M.C., Clem, W.C., Catledge, S.A., Xu, Y., Hennessy, K.M., Thomas, V., Jablonsky, M.J., Chowdhury, S., Stanishevsky, A.V., Vohra, Y.K., and Bellis, S.L. Mesenchymal stem cell responses to bone-mimetic electrospun matrices composed of polycaprolactone, collagen I and nanoparticulate hydroxyapatite. PLoS One **6,** e16813, 2011.
37. Ravichandran, R., Sundarrajan, S., Venugopal, J.R., Mukherjee, S., and Ramakrishna, S. Advances in polymeric systems for tissue engineering and biomedical applications. Macromol Biosci **12,** 286, 2012.
38. Han, J., Lazarovici, P., Pomerantz, C., Chen, X., Wei, Y., and Lelkes, P.I. Co-electrospun blends of PLGA, gelatin, and elastin as potential nonthrombogenic scaffolds for vascular tissue engineering. Biomacromolecules **12,** 399, 2011.
39. Almine, J.F., Bax, D.V., Mithieux, S.M., Nivison-Smith, L., Rnjak, J., Waterhouse, A., Wise, S.G., and Weiss, A.S. Elastin-based materials. Chem Soc Rev **39,** 3371, 2010.
40. Ji, W., Sun, Y., Yang, F., van den Beucken, J.J., Fan, M., Chen, Z., and Jansen, J.A. Bioactive electrospun scaffolds delivering growth factors and genes for tissue engineering applications. Pharm Res **28,** 1259, 2011.
41. Sahoo, S., Ang, L.T., Goh, J.C., and Toh, S.L. Growth factor delivery through electrospun nanofibers in scaffolds for tissue engineering applications. J Biomed Mater Res A **93,** 1539, 2010.

Address correspondence to:
Susan L. Bellis, PhD
Department of Cell, Developmental and Integrative Biology
University of Alabama at Birmingham
982A MCLM
1918 University Boulevard
Birmingham, AL 35294

E-mail: bellis@uab.edu

Received: October 16, 2013
Accepted: February 18, 2014
Online Publication Date: March 28, 2014